

S2TPVFormer: Spatio-Temporal Tri-Perspective View for temporally coherent 3D Semantic Occupancy Prediction

Sathira Silva^{1*} Savindu Wannigama^{1*} Gihan Jayatilaka² Roshan Ragel¹

¹Department of Computer Engineering, University of Peradeniya, Peradeniya 20400, Sri Lanka

²Department of Computer Science, University of Maryland, College Park, MD 20742, USA

{e17331, e17369}@eng.pdn.ac.lk; gihan@cs.umd.edu; roshanr@eng.pdn.ac.lk

Abstract

Holistic understanding and reasoning in 3D scenes play a vital role in the success of autonomous driving systems. The evolution of 3D semantic occupancy prediction as a pretraining task for autonomous driving and robotic downstream tasks captures finer 3D details compared to methods like 3D detection. Existing approaches predominantly focus on spatial cues, often overlooking temporal cues. Query-based methods tend to converge on computationally intensive Voxel representation for encoding 3D scene information. This study introduces S2TPVFormer, an extension of TPVFormer, utilizing a spatiotemporal transformer architecture for coherent 3D semantic occupancy prediction. Emphasizing the importance of spatiotemporal cues in 3D scene perception, particularly in 3D semantic occupancy prediction, our work explores the less-explored realm of temporal cues. Leveraging Tri-Perspective View (TPV) representation, our spatiotemporal encoder generates temporally rich embeddings, improving prediction coherence while maintaining computational efficiency. To achieve this, we propose a novel Temporal Cross-View Hybrid Attention (TCVHA) mechanism, facilitating effective spatiotemporal information exchange across TPV views. Experimental evaluations on the nuScenes dataset demonstrate a substantial 3.1% improvement in mean Intersection over Union (mIoU) for 3D Semantic Occupancy compared to TPVFormer, confirming the effectiveness of the proposed S2TPVFormer in enhancing 3D scene perception.

1. Introduction

Accurate and comprehensive 3D scene understanding and reasoning are pivotal for the development of robotic and autonomous driving systems. This reasoning spans two critical aspects: spatial reasoning and temporal reasoning. In

recent years, vision-centric 3D perception [3, 17, 12, 34, 29, 35] has gained significant interest as a promising alternative to LiDAR-based methods [13, 37, 24, 26] within the field of autonomous driving research. Vision-based approaches for 3D perception offer distinct advantages over LiDAR-based methods reliant on explicit depth measurements. Notably, vision-centric methods excel in identifying road elements, such as traffic lights and road signs, a task that proves challenging for LiDAR-based approaches. This combination of cost-effectiveness, long-range object detection, and the ability to recognize fine-grained road elements makes vision-centric 3D perception a valuable and promising approach in autonomous driving and robotics applications.

In the realm of vision-centric perception for autonomous driving systems, the utilization of multiple cameras has gained prominence in capturing both spatial and temporal cues from 2D RGB images. While single-camera methods [3, 35, 23, 25] offer a straightforward solution, they tend to process individual camera views independently, limiting their ability to capture and leverage information across multiple cameras. Consequently, they may struggle with recognizing all classes of objects in the real world. In contrast, multi-camera methods [6, 17, 12, 34, 29] have emerged as a compelling unified alternative, showcasing advancements in the realm of 2D-to-3D transformation.

For an extended period, one of the most popular 3D perception tasks has been 3D object detection [28, 31, 33, 17, 18, 11], estimating the locations and dimensions of objects and producing concise 3D bounding boxes for downstream tasks. However, object detection methods are constrained in terms of the expressiveness of their 3D bounding box outputs. With this objective, the primary emphasis of this paper is directed towards building a fine-grained 3D representation using 3D Semantic Occupancy (3D SOP). 3D semantic occupancy aims to capture intricate details of the surrounding scene, leveraging information derived from surrounding multi-camera images captured from different perspective views.

*Equal Contribution.

However, the previous works in 3D SOP literature [12, 34, 29, 35] seldom exploits temporal cues. This is evident in TPVFormer’s [12] SOP visualizations, where adjacent prediction frames lack temporal coherence as they rely solely on the current time step for semantic predictions. While previous works [17, 10, 14] emphasize the significance of temporal fusion in 3D object detection, earlier attempts at 3D SOP [12, 34, 29, 35] often overlooked the value of incorporating temporal information. Scene as Occupancy [27] utilizes BEVFormer’s spatiotemporal encoder and incorporates a complex decoder to reconstruct 3D features from spatiotemporal BEV features. However, lightweight decoder heads find appreciation in 3D perception literature for revealing the richness of the encoder’s embeddings and facilitating generalization, enabling easy adaptation of the encoder for diverse downstream tasks.

To overcome the aforementioned gaps in the literature, we propose **S2TPVFormer**, a spatiotemporal extension of TPVFormer [12]. In line with the principles of TPVFormer [12], we adopt TPV as the latent ego-space representation, benefiting from the strengths of both BEV and Voxel representations while maintaining computational efficiency. Our spatiotemporal encoder generates temporally rich S2TPV embeddings, predicting dense and temporally coherent 3D semantic occupancy through a lightweight MLP decoder. To achieve this, we leverage Spatial Cross-Attention (SCA) mechanism of TPVFormer without modification. Utilizing spatial fusion implemented through SCA as the basis, we introduce *Temporal Cross-View Hybrid Attention (TCVHA)* for temporal fusion, enabling spatiotemporal interactions across all TPV planes.

We recognize that the CVHA operation in TPVFormer essentially empowers the transformer to recognize the spatial interconnectedness of the three distinct embeddings, facilitating the exchange of geometrical information. Explicitly, it represents self-attention over TPV planes. However, implicitly, CVHA embodies a hybrid approach, combining self-attention and cross-attention across the three planes. Therefore, we acknowledge that this operation can be utilized for temporal fusion onto the TPV representation. Despite the information loss associated with warp-based temporal fusion, as highlighted in UniFusion [22], we adhere to the serial warp-based temporal fusion mechanism, similar to BEVFormer [17]. We argue that TCVHA enables the transformer to reconstruct lost information during warping while preserving computational efficiency.

To summarize, this work contributes in the following ways:

- We pioneer the use of TPV representation for embedding spatiotemporal information in 3D scenes within the domain of vision-centric SOP and the broader 3D perception literature.
- We introduce a novel temporal fusion workflow for TPV representation, analyzing how CVHA facilitates the sharing of spatiotemporal information across the three planes.
- Our method achieves a significant **3.1 %** improvement in mIoU for *3D SOP* as shown in Table 5 when evaluated on the nuScenes [2] validation dataset with TPVFormer’s [12] sparse pseudo-voxel ground truth, compared to TPVFormer.

2. Related Work

Vision-centric 3D Semantic Occupancy Prediction. The objective of 3D semantic occupancy prediction (*3D SOP*) is to intricately reconstruct the 3D environment surrounding an entity by incorporating detailed geometric information and semantic understanding. In the context of autonomous driving, 3D SOP serves as the academic alternative to occupancy networks [19]. This task shares a close relationship with Semantic Scene Completion (SSC) and *LiDAR Segmentation*, particularly when LiDAR serves as an additional input modality.

MonoScene [3] is a pioneering work in vision-based 3D perception, specifically focusing on Semantic Scene Completion (SSC). It introduces the first single-camera framework for SSC, enabling the reconstruction of outdoor scenes using RGB inputs alone. Building upon the foundation of MonoScene, TPVFormer [12], the first multi-camera method for 3D Semantic Occupancy Prediction, introduces a transformer-based TPV encoder. However, TPVFormer supervises its voxel predictions using pseudo-per-voxel labels generated from the sparse point cloud by assigning a new label of *empty* to any voxel that does not contain any point. A recent line of research [29, 27, 34] argues that dense semantic occupancy predictions require dense labels. They propose pipelines to generate densified ground-truth voxel semantics. With our method, we argue that densification of supervision is not the only way for high-quality SOP. Historical data also provide access to learn dense semantic occupancy.

Latent 3D Scene Representations. The effectiveness of 3D scene understanding heavily relies on the representation of the 3D environment, as illustrated in Figure 1. Traditional approaches [32, 25] involve dividing the 3D space into voxels and assigning each voxel a vector to denote its status. However, this representation proves computationally expensive. Alternatively, Bird’s Eye View (BEV) representation, which collapses the height information and focuses on the top-down view, offers a more efficient solution. While BEV-based methods [17, 11, 6, 16, 20, 21] perform remarkably well in tasks where height information is not very important, such as 3D object detection and map

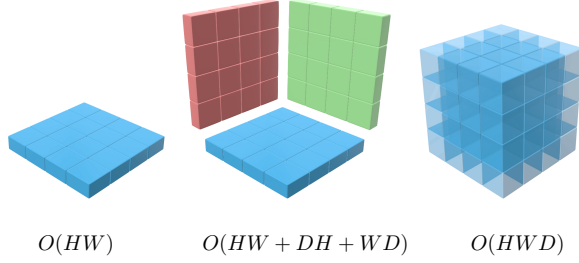


Figure 1. **Comparison of BEV, TPV [12], and Voxel latent vector fields used to represent 3D scenes.** While BEV is more efficient than the Voxel representation, it discards the height information and cannot provide a holistic understanding of a 3D scene. TPV is an approach to increase efficiency without compromising the loss of height information while being in the order of the same computational complexity as BEV representation.

segmentation, they struggle to encode the 3D structure of objects, thus hindering performance in 3D semantic occupancy prediction. Some 3D SOP methods [27] use BEV as the latent 3D scene embedding but have to employ complex decoders to reconstruct the lost height information from BEV. To overcome these limitations, TPVFormer [12] introduces a Tri-Perspective View (TPV) representation, generalizing the BEV representation by incorporating two additional orthogonal planes. This hybrid explicit-implicit representation [5, 4] aims to capture both the efficiency of BEV and the ability to encode the 3D structure of objects.

2D-3D Feature Lifting. Transforming 2D perspective observations into 3D space latent embeddings can be considered an ill-posed problem in a monocular setting due to the loss of depth information in 2D image formation. However, incorporating a strong *geometry prior* makes this task feasible. Monocular single-camera approaches address this challenge by predicting explicit depth maps [15, 21]. Nonetheless, depth estimations have limitations in capturing occlusions, rendering this method sensitive to the accuracy of depth measurements. In contrast, OFT [23] takes a different approach by not predicting depth. Instead, it directly copy-and-pastes the features in the image space to all locations that trace along the ray from the camera in the Bird’s Eye View (BEV) space.

On the other hand, LSS [21], a monocular multi-camera method proposes the LSS-based feature lifting method, which first “lift”s each perspective view image individually into a frustum of feature, then “splat”s all frustums into a rasterized BEV grid. In contrast to LSS-based methods [16, 11], an alternative approach [12, 17, 34, 22] uses a query-based approach while leveraging camera intrinsic and extrinsic parameters as a geometric prior to fuse spatial information from 2D multi-camera perspective views into a unified latent representation for ego-space. These meth-

ods employ attention mechanisms to learn the feature fusion mapping from multi-camera latent image spaces to the unified latent ego-space representation, that aligns with spatial ego-space. This process is commonly referred to as *spatial fusion*.

Temporal Reasoning. Temporal reasoning holds equal importance to spatial reasoning in a cognitive perception system. In human perception, temporal information is crucial for identifying occluded objects and determining the motion state of entities. A system proficient in spatiotemporal reasoning excels in making inferences with high temporal coherence.

Spatial fusion lays the groundwork for temporal fusion in the context of mainstream spatiotemporal methods [17, 10, 27, 36] employing a *warp-based temporal fusion* approach. BEVFormer [17] realizes temporal fusion via the concatenation of warped history BEV features with the BEV queries, followed by self-attention. Warping (in BEV) simply means aligning the history space according to ego-motion (yaw) at the present ego-space.

BEV warping could cause loss of information, and warping struggles to model long-range temporal fusion because it is usually serial. UniFusion [22] addresses this issue by introducing *virtual views* for parallel fusion. Despite its advantages, this approach is computationally intensive as spatial fusion is conducted across all fusion time steps, camera perspectives, and multi-scale feature levels.

3. Methodology

3.1. Overview

Our S2TPVFormer architecture, which follows the conventional structure of the transformer [30], as illustrated in Fig. 2 follows the basic pipeline of the *3D SOP* process mentioned in section 2. It consists of three major components, which are, the S2TPV Queries, Spatial Fusion via the SCA module, and Temporal Fusion via the Temporal CVHA module.

At timestamp t , the transformer encoder gets N_{cam} number of surround camera RGB images, \mathbf{I}_t as input and sends these images through the image backbone to extract multi-scale image features, $\mathbf{F}_t = \{\{F_t^{ij}\}_{i=1}^{N_{scale}}\}_{j=1}^{N_{cam}}$. Simultaneously, we preserve history BEV features at the prior timestamp $t - 1$, following BEVFormer [17]. The pipeline first uses the S2TPV queries, \mathbf{T}_t , to query temporal information from the preserved history BEV features, \mathbf{T}_{t-1}^{HW} . The Temporal CVHA module allows interactions between the three views as well as history views allowing them to exchange information among one another. Then, the S2TPV queries are used to perform spatial fusion using 2D feature maps \mathbf{F}_t via the Spatial Cross-Attention (SCA) module to adaptively lift 2D perspective features to

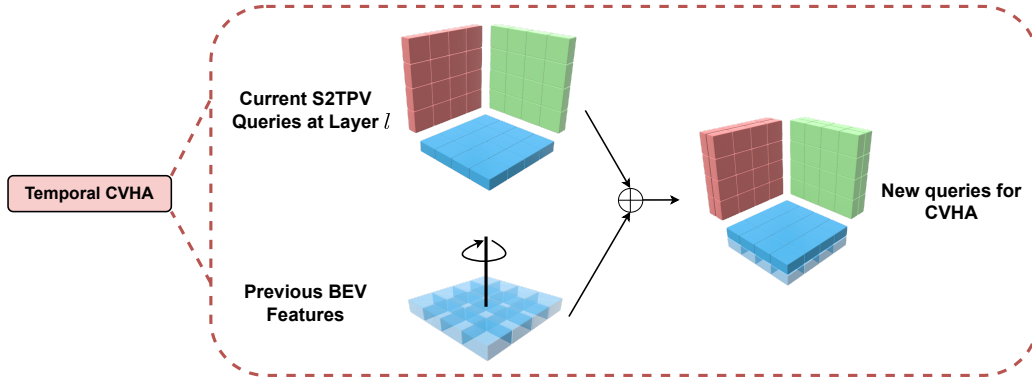
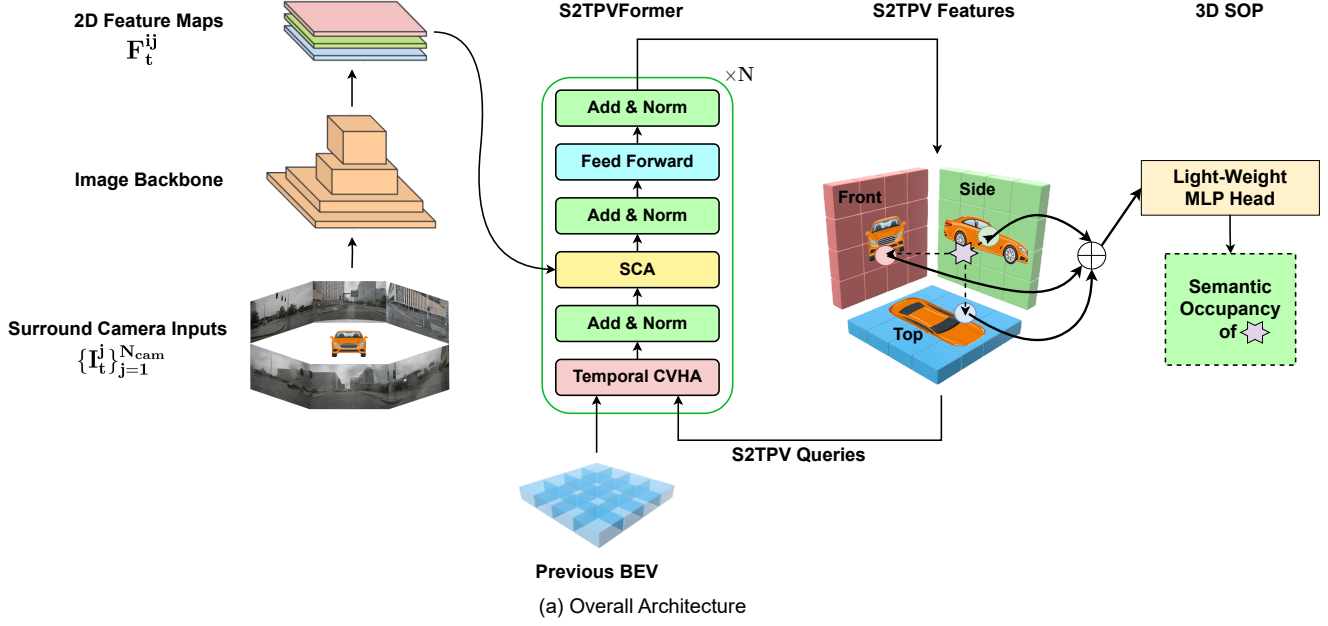


Figure 2. **The 3D SOP pipeline for the proposed S2TPVFormer architecture.** (a) First, we utilize an image backbone to extract 2D multi-scale feature maps. We adopt the spatial fusion mechanism of TPVFormer [12] to elevate 2D scene features to 3D TPV latent features. Subsequently, we employ Temporal Cross-View Hybrid Attention (TCVHA) to construct the S2TPV embeddings, enabling the interchange of these spatiotemporal features across the three planes. (b) Inspired by BEVFormer [17], we concatenate the warped (rotated and aligned with the current ego-space) BEV features from the previous time step with the S2TPV queries at the current layer, achieving temporal fusion.

the spatiotemporal S2TPV space, while using the camera intrinsic and extrinsic parameters as a geometry prior. The refined S2TPV feature outputs of each encoder layer are used as queries for the next encoder layer. After N such encoder layers, following TPVFormer [12], we use a lightweight prediction head over the aggregation of the broadcasted S2TPV features to predict the semantic occupancy in the voxel grid space, as described in Eq. 4.

S2TPV Queries. We utilize TPV as our 3D scene latent representation, drawing inspiration from TPVFormer [12].

This choice is motivated by the computational efficiency of TPV compared to Voxel representation and its capacity to capture fine-grained 3D structural information, in contrast to BEV. As depicted in Fig. 1, the storage and computational complexity of TPV fall between those of BEV and voxel representations. S2TPV (spatiotemporal TPV) features constitute the latent space of the temporally rich TPV embeddings generated by our S2TPVFormer encoder. S2TPV queries are a union of three predefined grid-shaped parameters representing each TPV plane,

$$\mathbf{T}_t = T_t^{HW} \cup T_t^{DH} \cup T_t^{WD} \quad (1)$$

Each S2TPV query maps to a 2D grid cell region of size $s \times s m^2$, where s is the spatial resolution of the voxel grid, extending from the view in the perpendicular direction in the corresponding real-world view. The S2TPV queries, implicitly stored in the model, essentially learn a set of latent spatiotemporal questions to ask for each spatial query from the model, facilitating the generation of temporally coherent 3D Semantic Occupancy. Similar to BEVFormer and TPVFormer, the S2TPV queries get progressively refined at each encoder layer where SCA lays down the spatial information, and TCVHA enhances them with temporal information. i.e. SCA provides the basis for TCVHA.

2D-to-3D Spatial Cross-Attention (SCA). We implement spatial fusion based on TPVFormer’s [12] Image Cross-Attention (ICA). The process involves expanding each 2D spatial query point on the TPV representation to a pillar of points orthogonal to the particular plane and uniformly sampling N_{ref} 3D reference points from it. These reference points are then projected onto the 2D camera perspective views using the camera’s extrinsic and intrinsic parameters. This 2D-3D lifting procedure establishes a geometry prior for the subsequent cross-attention mechanism. For the fusion, only the views that the projected 3D reference point, \mathbf{Ref}_j , hits are considered to further improve the computational efficiency. The actual spatial fusion is implemented using deformable attention [38], as described in Eq. 2, for computational efficiency, and the resulting fused features are a weighted summation over all views, determined by the computed attention for each hit view.

$$\text{DeformAttn}(q, p, x) = \sum_{i=1}^{N_{head}} W_i \sum_{j=1}^{N_{key}} A_{ij} \cdot W'_i x(p + \Delta p_{ij})$$

$$\text{SCA}(q, \mathbf{I}_t) = \frac{1}{|V_{hit}|} \sum_{j \in V_{hit}} \text{DeformAttn}(q, \mathbf{Ref}_j, I_t^j) \quad (2)$$

where V_{hit} denotes the set of hit camera views, $q \in \mathbb{R}^{C \times 1}$ where $q \in \mathbf{T}_t$, and I_t^j denotes the image features of the j^{th} camera view at timestamp t .

Temporal Cross-View Hybrid Attention. Despite having an efficient representation model, what TPVFormer [12] lacks is the temporal context in its latent TPV representation. TCVHA is the most essential component of the S2TPVFormer that helps embed spatiotemporal information in its latent representation. We implement temporal

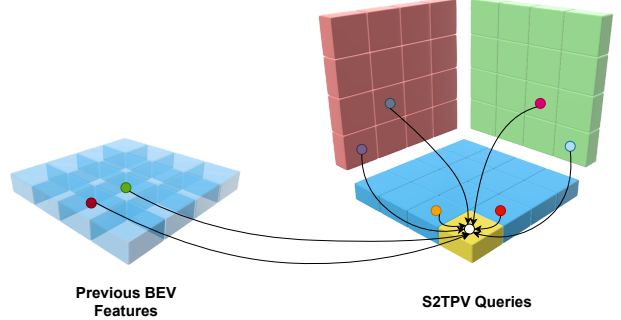


Figure 3. **TCVHA Spatiotemporal Interactions.** For a given BEV query feature q at a point $p = (h, w)$, it interacts with four types of feature points: (1) history points, (2) self points, (3) front view points, and (4) side view points. Temporal fusion is realized via the interactions with the history points. Even though a direct temporal fusion is not allowed for front and side views, CVHA interactions on them (not shown in this diagram) exchange the temporal information embedded in BEV with the front and side views.

fusion inspired by BEVFormer [17], that is, *warp-based temporal fusion*. We identify that there are three possible ways of fusing temporal information onto the TPV representation,

1. Warping and history concatenation are exclusively applied to the top view of the TPV representation, and Temporal Self-Attention (TSA) facilitates the fusion.
2. Warping and history concatenation are restricted to the top view, but TCVHA is employed for temporal fusion.
3. Warping and history concatenation are extended to all three planes, and TCVHA is employed for temporal fusion.

However, the implementation of (3) is not simply possible. Ego pitch and roll are usually neglected as they’re not significant. When considering the yaw, the Front and Side views of the TPV representation at timestamp $t - 1$ could occupy different slices of the ego-space at timestamp t since the axis of yaw is parallel to the Front and Side planes. Therefore, warping is only possible on the BEV plane.

Given the S2TPV queries at the current time step t and the preserved BEV features from time step $t - 1$, we align the historical BEV features T_{t-1}^{HW} before concatenating them with the T_t^{HW} queries, as illustrated in Fig. 2 (b). This alignment is performed based on the ego-motion, drawing inspiration from BEVFormer [17], to make the features at the same grid correspond to the same real-world location. For the Front and Side queries, they are doubled and concatenated, and, for the first run of the transformer, the BEV queries are also doubled and concatenated. These

new sets of queries, \mathbf{T}'_t , are used as the queries for computing TCVHA as follows.

$$\mathbf{T}'_t = [T_{t-1}^{HW'}; T_t^{HW}] \cup [T_t^{DH}; T_t^{DH}] \cup [T_t^{WD}; T_t^{WD}]$$

$$\text{TCVHA}(q'_{t,h,w}) = \text{DeformAttn}(q'_{t,h,w}, \mathbf{R}_{h,w}, \mathbf{T}'_t) \quad (3)$$

where $[x; y]$ denotes the concatenation of x and y along the channel dimension, and $q'_{t,h,w} \in \mathbb{R}^{2C \times 1}$ where $q'_{t,h,w} \in \mathbf{T}'_t$. Eq. 3 shows the TCVHA operation for the BEV plane. The CVHA reference points for deformable attention, $\mathbf{R}_{h,w}$, $\mathbf{R}_{d,h}$, and $\mathbf{R}_{w,d}$ are computed following TPVFormer.

TCVHA includes two CVHA operations that are performed parallelly with the queries \mathbf{T}'_t at the same time, over the current S2TPV embeddings \mathbf{T}_t , and aligned history S2TPV features \mathbf{T}'_{t-1} . The two attention outputs are then averaged to get the final output of TCVHA. How the TCVHA queries interact with the values is illustrated in Fig. 3. These interactions allow S2TPV feature embeddings to capture long-range temporal dependencies.

4. Experimental Setup and Implementation

4.1. Dataset

We use the nuScenes [2] dataset, which is a large-scale dataset designed for autonomous driving research and development. It provides 10,000 driving scenes in urban environments, including information captured in various weather conditions, times of day, and different urban environments across Boston and Singapore, which is split into 28,130 and 6,018 keyframes for training and validating respectively. Nuscenes includes data from monocular camera, LiDAR, RADAR and GPS. The dataset includes 1.1B LiDAR points manually annotated for 32 classes, which we use as ground truth labels to train our S2TPVFormer models for the 3D SOP and LiDAR Segmentation tasks. For our primary task of 3D SOP; we use camera and LiDAR inputs during training and camera-only during inference, and for the secondary task of LiDAR Segmentation we use in LiDAR inputs during both training and inference.

4.2. Hardware

We use 2 high-performance servers at the University of Peradeniya to train and validate our models; **(a) Turing** – has a Intel Core i9-13900K CPU with 32 cores, an NVIDIA GeForce RTX 3090 Ti GPU with 24 GB GPU memory, and 32 GB (2x16 GB) DDR5-6000 Memory, and **(b) Ampere** – has 2 Intel Xeon 4215R Processors with 32 cores, 2 RTX A6000 48GB GPUs, and 128 GB (8x16 GB) DDR4 2933

Memory. Table 1 shows the GPU usage during training and inferencing of different S2TPVFormer versions mentioned in Table 2, for the configurations defined in Table 3.

Model	base	small	tiny
S2TPVFormer01	-	13.8G	9.4G
S2TPVFormer03	36G	13.1G	9.3G
S2TPVFormer04	-	14.3G	10.4G
S2TPVFormer06	40G	14.3G	10.4G

Table 1. **GPU memory usage by S2TPVFormer version for different configurations during training.** All version-configuration pairs are trained on a single GPU with a batch size of 1.

4.3. Task Description

The fundamental concept behind 3D SOP involves the quantization of a physical 3D scene into a structured grid map (also known as an *occupancy network*), assigning semantic labels to each cell. Formally, the task requires predicting a semantic label for all voxels within this predefined grid of size $H \times W \times D$ based on the information derived from surrounding multi-camera images. The problem can be formulated as shown in Eq. 4.

$$V = \phi \left(\{I_j\}_{j=1}^{N_{cam}} \right) \quad (4)$$

where $\{I_j\}_{j=1}^{N_{cam}}$ are the N_{cam} number of multi-camera images, ϕ is a neural network, and $V \in \mathbb{R}^{L \times H \times W \times D}$ is the semantic occupancy prediction for a voxel in the grid for L number of semantic labels. A voxel semantic encapsulates two essential aspects: the *occupancy state* and the *semantic content*. The occupancy state can manifest as *free space*, *occupied*, or *out-of-vocabulary*, and this is achieved by utilizing *empty* and *noise* as additional semantic labels, representing free and out-of-vocabulary occupancy states, respectively. Broadly, the voxel semantics are of two types: background voxels (*free space*) and foreground voxels (*semantic labels*).

4.4. Training for 3D Semantic Occupancy Prediction and LiDAR Segmentation

4.4.1 Occupancy as a Ground Truth Label

In addition to the obvious difference between these two tasks; which is predicting the occupancy and semantics of voxels *vs* semantics of LiDAR points, the other major difference is how we supervise the model during training. When we don't supervise the *empty* class label, and instead, only supervise the other known classes during training, the model does not learn to predict the occupancy in the

concerned surrounding 3D space. Therefore intuitively the model only learns to predict the semantic classes for voxels and/or LiDAR points.

4.4.2 Formation of Voxel Ground Truth Labels

We supervise the model during training using a set of pseudo-per-voxel labels. These labels are generated with the help of labeled sparse LiDAR points provided in the nuScenes dataset [2]. We first initialize all the voxels with the *empty* class label. Then we label the voxels with the label of the LiDAR point(s) falling inside each voxel, so that the voxels containing LiDAR points will be labeled with the semantic class of the LiDAR point as occupied, and voxels that do not contain a LiDAR point will retain its initialized *empty* class label implying it is not occupied.

4.4.3 Loss Functions

We use two loss functions for supervision during training; (a) **Cross-entropy loss** to improve voxel classification accuracy and avoid semantic ambiguity, and (b) **Lovasz-softmax loss** [1] to maximize the IoU score for classes. For both *3D SOP* and *LiDAR Segmentation* tasks we use voxel predictions as inputs to both loss functions. and losses. TPVFormer [12] in their ablation study shows that using LiDAR point predictions as inputs to the Lovasz-softmax loss, voxel prediction as inputs to the cross-entropy loss gives the best results for the *LiDAR Segmentation* task, but we do not adapt this approach as our objective of performing *LiDAR Segmentation* as a secondary task is to understand the generalization capability of the S2TPVFormer architecture.

In chapter 5 we see that the general trend is to get better validation metric values for *LiDAR Segmentation* experiments. This is justified by the following facts; (a) In general, the majority of surrounding space for a given scene is empty space, and, (b) Since we are using LiDAR points as ground truth, we get a sparse set of ground truth points which further increases the number of *empty* class labels given as supervision during training. These two facts are sufficient to argue that *empty* is the most prominent semantic class observed and predicted by the model, and that this is the reason why get relatively higher validation metric values for *LiDAR Segmentation* experiments compared *3D SOP* when trained for the same number of epochs.

4.5. Implementation Details

We implement five versions of S2TPVFormer shown in Table 2, which differ based on the degree of temporal fusion and the level of interaction among the three TPV planes in the latent representation of the encoder. All versions use the same decoder head which is a lightweight

Model	CVHA	Temporal Attention
S2TPVFormer01	No	No
S2TPVFormer02	Yes	No
S2TPVFormer03	No	BEV
S2TPVFormer04	Yes	TPV
S2TPVFormer06	Yes	BEV

Table 2. Five versions of S2TPVFormer models.

MLP instantiated with two linear layers and an intermediate activation layer. This lightweight decoder is applied to voxel and LiDAR point features to predict their semantic labels. The inclusion of a lightweight MLP, as opposed to involving a complex decoder as in OccNet [27], aims to demonstrate the superiority of our encoder. We use two image backbones for different configurations defined in Table 3; S2TPVFormer-base uses the ResNet101-DCN [7] initialized from FCOS3D [31] checkpoint, while all other configurations use ResNet50 [9] pretrained on the ImageNet dataset [8].

S2TPVFormer01 and **S2TPVFormer02** are the most basic versions of S2TPVFormer. Both versions do not use temporal attention, and therefore the module reduces down to deformable self-attention over BEV, and TPV planes respectively, as mentioned in section 3.1. S2TPVFormer01 is functionally equivalent to the TPVFormer04 version introduced by TPVFormer [12]. We use these versions as benchmarks to compare with other versions of S2TPVFormer that use temporal attention.

To comprehensively understand the effect of temporal attention on *3D SOP* and *LiDAR Segmentation*, we gradually introduced the use of temporal attention with the following versions; **S2TPVFormer03** is the first version in which we introduce the temporal attention module for the tri-perspective view architecture. So as the first step, we introduce temporal attention explained in section 3.1, only to the BEV plane out of the three TPV planes. Given that we do not use CVHA in this version, disabling the exchange of information among the three planes. So it is reasonable to argue that only the BEV plane would carry temporal information, while the other two planes would contain queries regarding the instantaneous spatial information.

With **S2TPVFormer06**, we go one step further and introduce CVHA allowing the information among the three TPV planes, but we retain the temporal attention

Model Config	Embedding Dimensionality	TPV Resolution	Backbone	Image Resolution
S2TPVFormer-base	256	200x200x16	ResNet101	1600x900
S2TPVFormer-medium	256	100x100x8	ResNet50	1600x900
S2TPVFormer-small	128	100x100x8	ResNet50	1600x900
S2TPVFormer-tiny	128	100x100x8	ResNet50	1200x675

Table 3. Model configurations used to run experiments.

only on the BEV plane. So intuitively, we allow the BEV plane queries to explicitly learn temporal information, while allowing the other two planes to implicitly learn temporal information from the BEV plane via CVHA.

With **S2TPVFormer04** we increase the degree of temporal attention another step further by implementing temporal attention on all three TPV planes. As described in Section 3.1, aligning the past side and front planes from different timesteps cannot be done as accurately as we do for the BEV plane. So it is arguable that the temporal fusion on those two planes would not be as accurate as the temporal fusion on the BEV plane. We also argue that due to the exchange of information among the three planes via CVHA, this error on the front and side planes could be rectified up to a certain extent.

5. Results and Analysis

5.1. Evaluation Metrics

For 3D perception tasks such as *LiDAR Segmentation* and *3D SOP*, Intersection over Union (IoU) defined by Eq. 5 and mean Intersection over Union (mIoU) defined by Eq. 6 stand as significant validation metrics to measure model accuracy. IoU measures the overlap between predicted and ground truth bounding boxes or segmented regions, offering a precise assessment of localization accuracy. A higher IoU signifies better alignment between predicted and actual boundaries. Complementing this, mIoU calculates the average IoU across multiple classes, providing an overall performance indicator.

$$IoU = \frac{TP}{TP + FP + FN} \quad (5)$$

$$mIoU = \frac{1}{C} \sum_{c=1}^C \frac{TP_c}{TP_c + FP_c + FN_c} \quad (6)$$

5.2. Analysis of 3D Semantic Occupancy Prediction Results

5.2.1 Quantitative Analysis

One of our main objectives of developing S2TPVFormer is to beat the validation metrics of the TPVFormer04 version of TPVFormer [12], by introducing the new temporal attention module. Therefore as our initial experiment, we train the TPVFormer04 model for the S2TPVFormer-tiny configuration defined in Table 3, on the nuScenes train dataset for 6 epochs to compare with the results of S2TPVFormer versions at the same number of epochs. The results in the Table 4 show that we get approximately equal results for both **TPVFormer04** and **S2TPVFormer01** versions, providing evidence that these two models are functionally equivalent.

S2TPVFormer03 shows an improvement of 1.1 % compared to TPVFormer04 providing evidence that even taking temporal attention only on the BEV plane significantly improves the performance. **S2TPVFormer06**, which shows an even better result with an improvement of 2.6 % compared to TPVFormer04, proves that increasing the degree of temporal fusion increases the performance of the model. **S2TPVFormer04** too shows an improvement of 0.3 % compared to TPVFormer04, but this improvement is less than the one we observe for S2TPVFormer03. This trend of results we see in Table 4, agrees with the theoretical explanation we provide in section 4.5, and encourages our understanding and explanation of how the temporal attention module functions, and how different degrees of temporal fusion improves the model performance accordingly.

In addition to the experiments in Table 4, we train the TPVFormer04 and S2TPVFormer03 models for the S2TPVFormer-small-plus configuration defined in Table 3. The motivation behind this experiment, shown in Table 5 is two-fold; (a) We argue that using the original image resolution and a higher embedding dimensionality would show a higher variation in the validation metrics when we run experiments with varying hyper-parameters

Method	mIoU	barrier	bicycle	bus	car	const. veh.	motorcycle	pedestrian	traffic cone	trailer	truck	drive. surf.	other flat	sidewalk	terrain	manmade	vegetation
TPVFormer*	36.3	51.7	8.3	47.0	59.6	10.4	18.3	22.7	9.3	12.5	47.1	81.5	48.5	47.2	45.4	33.0	37.8
S2TPVFormer03	37.4	49.4	6.9	52.7	59.4	22.2	14.9	20.7	11.2	18.6	52.6	81.9	48.3	47.9	48.2	32.6	30.1
S2TPVFormer06	38.9	51	6.1	65.5	60.4	23.8	11.5	24.2	10.3	21.4	55	83.8	49.0	48.5	48.2	32.2	32
S2TPVFormer04	36.6	46.5	4.3	65.4	56.6	9.2	12.5	17.8	11	21.6	53.8	82.2	45.8	46.5	48.1	29.8	35.1

Table 4. **3D Semantic Occupancy Prediction Results on the nuScenes validation set for S2TPVFormer-tiny configuration defined in table 3.** All models are trained for 6 epochs. The results for each model in the table are for the checkpoint that gives the best validation results out of the 6 epochs trained. For a fair comparison, we use the same settings as in our S2TPVFormer-tiny configuration, which is denoted as TPVFormer*.

Method	mIoU	barrier	bicycle	bus	car	const. veh.	motorcycle	pedestrian	traffic cone	trailer	truck	drive. surf.	other flat	sidewalk	terrain	manmade	vegetation
TPVFormer*	39.0	54.2	5.4	58.1	67.0	30.9	17.2	21.4	11.1	19.7	53.7	76.3	48.2	50.9	49.1	28.4	32.1
S2TPVFormer03	42.1	54.3	5.2	61.8	65.2	28.6	26.3	22.7	9.7	36.6	57.9	83.2	49.9	49.3	49.3	37.2	36.8

Table 5. **3D Semantic Occupancy Prediction Results on the nuScenes validation set for S2TPVFormer-medium configuration defined in table 3.** Both models are trained for 5 epochs. The results for each model in the table are for the checkpoint that gives the best validation results out of the 5 epochs trained. For a fair comparison, we use the same settings as in our S2TPVFormer-medium configuration, which is denoted as TPVFormer*.

during the ablation study, and thereby better reflect the effect of those hyper-parameters to the *3D SOP* task using S2TPVFormer. (b) We choose the two models TPVFormer04 and S2TPVFormer03 for this experiment, as the only functional difference between these two models is the novel temporal attention module for S2TPVFormer which we introduce in this paper.

From the data in Table 5, S2TPVFormer03 shows a 3.1% improvement in the mIoU when trained for the S2TPVFormer-small_plus configuration, as opposed to the 1.1% improvement we see in Table 4 when trained for the S2TPVFormer-tiny configuration. In light of this, we argue that we will be able to get an even better improvement for S2TPVFormer if we train the models for higher configurations.

5.3. Analysis of LiDAR Segmentation Results

5.3.1 Quantitative Analysis

We carry out a set of experiments for the task of LiDAR segmentation using all the S2TPVFormer versions to test for the generalization capability of our model, especially of the novel temporal attention module for S2TPVFormer.

Table 7 shows the validation results for versions of

Ablation	Embed Dim	TPV Resolution	mIoU
-	256	100x100x8	42.1
1	256	200x200x16	40.5
2	128	200x200x16	38.0

Table 6. **Summary of the ablation study on 3D SOP for S2TPVFormer03.** All other hyper-parameters are kept constant. All experiments are trained for 5 epochs. The results for all studies in the table are for the checkpoint that gives the best validation results out of the 5 epochs trained.

S2TPVFormer after training for a single epoch. The 1.3% increase in the mIoU of **S2TPVFormer02** when compared to **S2TPVFormer01** is evidence that LiDAR segmentation favors CVHA. The 5.5% improvement for **S2TPVFormer03** for the same comparison shows the significance of the temporal attention module for the LiDAR segmentation task, and the 6.3% improvement for **S2TPVFormer06** gives us reason to conclude that CVHA in S2TPVFormer06 has facilitated BEV plane to share the temporal information it learns with the front and the side planes. The mIoU for **S2TPVFormer04** is higher than that

S2TPVFormer01 and S2TPVFormer02, but considerably lower than that of S2TPVFormer03 and S2TPVFormer06. This proves that the problem with aligning front and end planes from different time steps, which is explained in section 3.1, causes the model to learn inaccurate temporal information.

5.3.2 Ablation Study

During this ablation study, we aim to understand the effect of the TPV resolution, embedding dimensionality, and the range of temporal attention on *LiDAR Segmentation*. We change only the mentioned hyper-parameters and keep all other hyper-parameters constant at values defined for S2TPVFormer-small in Table 3. We can observe from the results in Table 8 that having a higher embedding dimensionality and TPV resolution is favorable for LiDAR segmentation. Also, the 8.9% improvement in ablation 2 where we increase the TPV resolution, compared to the 3.6% improvement in ablation 1 where we increase the embedding dimensionality shows that S2TPVFormer favors resolution over embedding dimensionality for LiDAR segmentation. This is the same observation that TPVFormer [12] gets during their ablation study for LiDAR segmentation. So we can conclude that adding the temporal attention module does not change the overall effect of these two hyper-parameters.

Increasing the range of temporal attention could be considered the most important ablation study we do since the temporal attention module is our most important novel contribution in this paper. As discussed in section 3.1, by default we randomly choose 3 samples from the consecutive sequence of the immediate past 2 seconds (4 frames sampled at 2 Hz) to take temporal attention, but during this ablation study we increase this temporal attention range to randomly choosing 6 samples from the consecutive sequence of the immediate past 4 seconds (8 frames sampled at 2 Hz), and we achieve an improvement of 2.5% for the mIoU during this study.

We get our inspiration for the novel temporal attention module from BEVFormer [17]. In the ablation study on the map segmentation task done by Unifusion [22], they show that BEVFormer [17] shows the highest performance when taking temporal attention over 3 fusion steps, and further increasing the range of temporal attention decreases performance. In our ablation, we show that increasing the number of fusion steps from 3 to 6 increases the performance of S2TPVFormer, showing the possibility of a longer range of temporal fusion compared to BEVFormer. We argue that the reason for this is the use of 3 TPV planes in the latent representation of S2TPVFormer as opposed to the single BEV plane used by BEVFormer, which allows the model to learn and remember more information from a longer range

of temporal fusion.

6. Conclusion

In this paper, we delve into the potential of exploiting spatiotemporal intricacies in the TPV representation to enhance the temporal coherence of 3D Semantic Occupancy Prediction within the existing TPVFormer architecture. We are pioneers in implementing this enhancement, aiming to elevate the model’s ability to understand the 3D scene over time. Leveraging 2D-3D spatial cross-attention, we lift multi-camera scene features to 3D scene features, forming the groundwork for effective temporal fusion across TPV planes. With the support of Cross-View Hybrid Attention, this approach significantly advances the TPVFormer’s present performance in 3D perception.

Limitations and Future directions. While our method enhances the quality of 3D SOP compared to TPVFormer, S2TPVFormer does not fully exploit temporal information to its maximum potential. Warp-based temporal fusion in S2TPVFormer sacrifices accurate and lossless temporal fusion for computational efficiency. Additionally, serial warping treats all timestamps equally, when, in fact, they should be assigned different weights for effective long-range temporal fusion. Hence, there is still room for enhancements in S2TPVFormer, aligning with the approach seen in UniFusion [22].

References

- [1] Maxim Berman, Amal Rannen Triki, and Matthew B Blaschko. “The lovász-softmax loss: A tractable surrogate for the optimization of the intersection-over-union measure in neural networks”. In: *Proceedings of the IEEE conference on computer vision and pattern recognition*. 2018, pp. 4413–4421.
- [2] Holger Caesar et al. “nuScenes: A multimodal dataset for autonomous driving”. In: (Mar. 2019).
- [3] Anh-Quan Cao and Raoul de Charette. “MonoScene: Monocular 3D Semantic Scene Completion”. In: *CVPR*. 2022.
- [4] Eric R. Chan et al. “Efficient Geometry-aware 3D Generative Adversarial Networks”. In: 2022.
- [5] Anpei Chen et al. “TensorRF: Tensorial Radiance Fields”. In: 2022.
- [6] Kashyap Chitta, Aditya Prakash, and Andreas Geiger. “NEAT: Neural Attention Fields for End-to-End Autonomous Driving”. In: *International Conference on Computer Vision (ICCV)*. 2021.
- [7] Jifeng Dai et al. “Deformable Convolutional Networks”. In: *Proceedings of the IEEE International Conference on Computer Vision (ICCV)*. Oct. 2017.

Method	mIoU	barrier	bicycle	bus	car	const. veh.	motorcycle	pedestrian	traffic cone	trailer	truck	drive. surf.	other flat	sidewalk	terrain	manmade	vegetation
S2TPVFormer01	34.3	35.6	0.0	27.5	51.1	24.7	7.1	14.0	4.4	33.1	41.7	79.3	16.1	37.3	46.5	65.4	64.6
S2TPVFormer02	35.6	44.5	0.2	26.1	56.7	17.4	8.2	15.5	4.0	29.6	43.0	81.3	35.5	36.3	44.2	62.4	64.3
S2TPVFormer03	39.8	40.7	6.4	56.8	57.6	24.2	12.1	19.5	8.3	23.8	44.3	80.8	39.8	38.0	49.7	65.8	68.9
S2TPVFormer06	40.6	45.5	7.9	51.0	54.6	29.7	6.9	15.7	5.2	36.4	51.0	82.3	39.6	41.3	49.1	68.7	64.3
S2TPVFormer04	37.9	40.1	3.6	41.6	53.2	24.6	6.9	19.4	7.3	43.2	37.7	82.3	37.3	37.9	41.7	66.4	62.7

Table 7. *LiDAR Segmentation Results on the nuScenes validation set for S2TPVFormer-small configuration defined in table 3.* All models are trained for 1 epoch.

Ablation	Embed Dim	TPV Resolution	Time Range	mIoU
-	128	100x100x8	3s_4t	39.8
1	256	100x100x8	3s_4t	43.4
2	128	200x200x16	3s_4t	48.7
3	128	100x100x8	6s_8t	42.3

Table 8. *Summary of the ablation study on LiDAR Segmentation for S2TPVFormer03.* All other hyper-parameters are kept constant. All experiments are trained for 1 epoch.

- [8] Jia Deng et al. “Imagenet: A large-scale hierarchical image database”. In: *2009 IEEE conference on computer vision and pattern recognition*. Ieee. 2009, pp. 248–255.
- [9] Kaiming He et al. “Deep residual learning for image recognition”. In: *Proceedings of the IEEE conference on computer vision and pattern recognition*. 2016, pp. 770–778.
- [10] Junjie Huang and Guan Huang. “BEVDet4D: Exploit Temporal Cues in Multi-camera 3D Object Detection”. In: *arXiv preprint arXiv:2203.17054* (2022).
- [11] Junjie Huang et al. “BEVDet: High-performance multi-camera 3D object detection in Bird-Eye-View”. In: (Dec. 2021).
- [12] Yuanhui Huang et al. “Tri-Perspective View for Vision-Based 3D Semantic Occupancy Prediction”. In: 2023.
- [13] Alex H. Lang et al. “PointPillars: Fast Encoders for Object Detection from Point Clouds”. In: 2019.
- [14] Qi Li et al. *HDMaNet: An Online HD Map Construction and Evaluation Framework*. 2021.
- [15] Yiming Li et al. “VoxFormer: Sparse Voxel Transformer for Camera-based 3D Semantic Scene Completion”. In: 2023.
- [16] Yin hao Li et al. “BEVDepth: Acquisition of reliable depth for multi-view 3D object detection”. In: (June 2022).
- [17] Zhiqi Li et al. “BEVFormer: Learning bird’s-eye-view representation from multi-camera images via spatiotemporal transformers”. In: (Mar. 2022).
- [18] Yingfei Liu et al. “PETR: Position embedding transformation for multi-view 3D object detection”. In: (Mar. 2022).
- [19] Lars Mescheder et al. *Occupancy Networks: Learning 3D Reconstruction in Function Space*. 2019.
- [20] Chen Min et al. “Occ-BEV: Multi-Camera Unified Pre-training via 3D Scene Reconstruction”. In: 2023.
- [21] Jonah Philion and Sanja Fidler. “Lift, splat, shoot: Encoding images from arbitrary camera rigs by implicitly unprojecting to 3D”. In: (Aug. 2020).
- [22] Zequn Qin et al. “UniFusion: Unified multi-view fusion transformer for spatial-temporal representation in bird’s-eye-view”. In: (July 2022).
- [23] Thomas Roddick, Alex Kendall, and Roberto Cipolla. “Orthographic Feature Transform for Monocular 3D Object Detection”. In: 2018.
- [24] Luis Roldão, Raoul de Charette, and Anne Verroust-Blondet. “LMSCNet: Lightweight Multiscale 3D Semantic Completion”. In: (Aug. 2020).
- [25] Danila Rukhovich, Anna Vorontsova, and Anton Konushin. “ImVoxelNet: Image to Voxels Projection for Monocular and Multi-View General-Purpose 3D Object Detection”. In: 2021.
- [26] Shaoshuai Shi, Xiaogang Wang, and Hongsheng Li. “PointRCNN: 3D object proposal generation and detection from point cloud”. In: (Dec. 2018).
- [27] Chonghao Sima et al. “Scene as Occupancy”. In: (2023).
- [28] Andrea Simonelli et al. “Disentangling monocular 3D object detection”. In: (May 2019).

- [29] Xiaoyu Tian et al. “Occ3D: A Large-Scale 3D Occupancy Prediction Benchmark for Autonomous Driving”. In: 2023.
- [30] Ashish Vaswani et al. “Attention Is All You Need”. In: 2017.
- [31] Tai Wang et al. “FCOS3D: Fully convolutional one-stage monocular 3D object detection”. In: (Apr. 2021).
- [32] Yan Wang et al. “Pseudo-LiDAR from Visual Depth Estimation: Bridging the Gap in 3D Object Detection for Autonomous Driving”. In: 2020.
- [33] Yue Wang et al. “DETR3D: 3D Object Detection from Multi-view Images via 3D-to-2D Queries”. In: (Oct. 2021).
- [34] Yi Wei et al. “SurroundOcc: Multi-Camera 3D Occupancy Prediction for Autonomous Driving”. In: 2023.
- [35] Yunpeng Zhang, Zheng Zhu, and Dalong Du. “OccFormer: Dual-path Transformer for Vision-based 3D Semantic Occupancy Prediction”. In: 2023.
- [36] Yunpeng Zhang et al. “BEVerse: Unified Perception and Prediction in Birds-Eye-View for Vision-Centric Autonomous Driving”. In: 2022.
- [37] Xinge Zhu et al. “Cylindrical and asymmetrical 3D convolution networks for LiDAR-based perception”. In: (Sept. 2021).
- [38] Xizhou Zhu et al. “Deformable DETR: Deformable Transformers for End-to-End Object Detection”. In: 2021.